High tensile strength and transformation-induced plasticity in bulk polycrystalline omega titanium

Norimasa Nishiyama[1,2,3*], Yoshinori Tange[1], Takashi Sawahata[2], Masafumi Matsushita[4], Kazuya Tokuda[5], Kosuke Tominaga[5], Takashi Sekiya[5], Koji Kuramochi[5], Keita Sasaki[1], Fumihiro Wakai[2], Zenji Horita[6,7,8], Yutaka Kobayashi[1], Akio Fujimura[1]

1: Advanced Materials Laboratory, Sumitomo Electric Industries, Ltd, 1-1-1 Koyakita, Itami 664-0016, Japan

2: Laboratory for Materials and Structures, Tokyo Institute of Technology, R3-22, 4259 Nagatsuta-cho, Midori-ku, Yokohama 226-8503, Japan

3: Research Center for Materials Nanoarchitectonics, National Institute for Materials Science, 1-1 Namiki, Tsukuba 305-0044, Japan

4: Department of Mechanical Engineering, Ehime University, 3 Bunkyo-cho, Matsuyama 790-8577, Japan

5: Analysis Technology Research Center, Sumitomo Electric Industries, Ltd, 1-1-1 Koyakita, Itami 664-0016, Japan

6: School of Engineering, Kyushu Institute of Technology, 1-1 Sensui-cho, Tobata-ku, Kitakyushu 804-8550, Japan

7: Magnesium Research Center, Kumamoto University, 2-39-1 Kurokami, Chuo-ku Kumamoto 860-8555, Japan

8: Synchrotron Light Application Center, Saga University, 1 Honjo-machi, Saga, 840-8502, Japan

*Corresponding author: Norimasa Nishiyama

Present affiliation: Research Center for Materials Nanoarchitectonics, National Institute for Materials Science, 1-1 Namiki, Tsukuba 305-0044, Japan

Email: nishiyama.norimasa@nims.go.jp

Abstract

Titanium and its alloys exhibit advantageous ductility and strength-to-weight ratios, which makes them suitable for use as structural materials in numerous industrial applications. The ω phase has been observed to precipitate during the aging process of titanium alloys, resulting in a loss of ductility. Here we report tensile behavior of bulk polycrystalline ω-titanium with a chemical composition of commercially pure titanium grade 4 and an average grain size of 3.4 μm. We observed that stress-induced ω → α martensitic phase transformation occurs exclusively in the plastic regime. As plastic deformation proceeds, the volume fraction of α-phase increases. The 0.2% offset yield strength, tensile strength, and elongation to failure were determined to be 1130 ± 30 MPa, 1220 ± 30 MPa, and 16 ± 2 %, respectively. The present study revealed transformation-induced plasticity in this material. The mechanical properties of this material with the pure titanium composition are comparable to those of a titanium alloy Ti-6Al-4V. The bulk polycrystalline ω-titanium can potentially be utilized for biomedical applications, such as dental implants.

Keywords:

Titanium; ω phase; high-pressure and temperature; tensile strength; martensitic transformation; transformation-induced plasticity

Introduction

Titanium exhibits three major phases, designated as α, β, and ω phases, which vary according to pressure and temperature[1]. At ambient conditions, the substance stabilizes in a hexagonal closed-packed (hcp) structure, designated as the α phase. However, at ambient pressure and temperatures greater than 1155 K, the α phase undergoes a phase transition to a body-centered cubic (bcc) structure, which is designated as the β phase. Moreover, under conditions of high pressure, the α phase transforms into a simple hexagonal structure, referred to as the ω phase[2]. The ω phase is stable at least up to 100 GPa and it further transforms into high-pressure phases, called γ and δ phases[3,4].

The occurrence of metastable ω phase in β-Ti alloys has been observed at ambient pressure after heat treatment and aging process[5,6]. The presence of metastable ω phase has been shown to have a significant impact on the mechanical properties of these alloys, causing substantial increases in strength and significant reductions in ductility[7], or, in some cases, leading to a complete loss of ductility[8,9]. The embrittlement phenomenon associated with the ω phase[10] has posed a significant challenge to the utilization of these alloys in safety-critical applications such as medical devices. Consequently, numerous studies have been conducted to suppress the formation of ω phase[11,12]. Recently, new approaches have emerged to overcome this problem by controlling the growth of the ω phase during aging and by preserving the β matrix stability. These attempts have enhanced the strength through

nanoprecipitation of the ω phase while maintaining good ductility by preserving the TRIP/TWIP effect, particularly in Ti-12Mo alloy[13,14]. Understanding the basic properties of the ω-phase is crucial for improving the mechanical properties of Ti alloys.

In order to measure the fundamental properties of the ω phase, studies have been conducted on the fabrication of polycrystalline titanium materials consisting primarily of the ω phase. Pioneering work in this field was performed by Todaka et al[15], who employed high-pressure torsion (HPT) processing at 5 GPa and room temperature (30˚C) to severely deform a pure α-titanium specimen. Consequently, the authors obtained 90 mass% polycrystalline ω phase with a grain size measured in hundreds nanometers. The Vickers hardness of this material was reported to be 3.7 GPa, a value that exceeds that of α-titanium. Tane et al.[16] employed the same technique to produce polycrystalline pure titanium specimens consisting exclusively of the ω phase. A complete set of elastic stiffness of the ω phase was measured, and the reported values were found to be consistent with those predicted by theoretical calculations[17]. Two other studies employed a static high-pressure technique to fabricate bulk polycrystalline specimens consisting of a single-phase of the ω phase in pure titanium. Li et al.[18] fabricated a specimen with dimensions of 3 × 3 × 4 mm^3 under 12.2 GPa and room temperature. The authors reported the Vickers hardness to be 2.5 GPa and the measured elastic moduli are consistent with those reported by Tane et al[16]. Sawahata et al[19] fabricated rod-shaped specimens with a diameter of 4 mm and a height of 3 mm under simultaneous

high pressure (12 GPa) and high temperature (400˚C). The uniaxial compressive stress-strain relationship was obtained and the 0.2% offset yield strength was determined to be 913 MPa. The bulk polycrystalline ω-Ti material was reported to be more than twice as strong as the α phase[19]. However, the tensile behavior of this material has never been observed.

In the present study, tensile tests were performed on bulk polycrystalline ω titanium materials that were fabricated in the thermodynamic stability field under high-pressure and high-temperature (high-*PT*) conditions. The stress-strain curves were obtained, and the data were analyzed to determine yield strength, tensile strength, and elongation to failure. Time-resolved X-ray diffraction measurements were also carried out during tensile tests using synchrotron radiation. We observed that the ω phase transforms into the α phase during plastic deformation.

Results and discussion

In this study, four types of pure titanium materials (α-Ti) were utilized as starting materials to fabricate bulk polycrystalline ω titanium materials (ω-Ti materials) under high-*PT*: titanium with purity of 99.999 wt% metals basis (5N) (0.02 wt% oxygen); commercially pure titanium grade 2 (CP-Ti Grade 2) (0.12 wt% oxygen); CP-Ti Grade 4 (0.38 wt% oxygen); cold-worked CP-Ti Grade 4 (0.37 wt% oxygen). The minor element contents of these CP-Ti materials are given in Supplementary Table 1. In each case, the presence of

single phase ω was confirmed by X-ray diffraction measurements (XRD) after the high-*PT* treatment (Figs. 1a-d). It is noteworthy that despite the literature on the blocking of the martensitic α → ω transformation by certain impurities[15,20-22], CP-Ti Grade 4 readily transformed to the ω phase in the high-*PT* treatment. The microstructures of the ω-Ti materials were examined using field-emission scanning electron microscopy (FESEM) with an electron backscatter diffraction (EBSD) detector. The obtained images demonstrate a decrease in grain size with increasing impurity content (Figs. 1e-g). The ω-Ti material exhibiting the smallest grain size (Fig. 1h) was fabricated by utilizing cold-worked CP-Ti Grade 4 as the starting material and by minimizing the duration of heating under high pressure (Supplementary Figure 1).

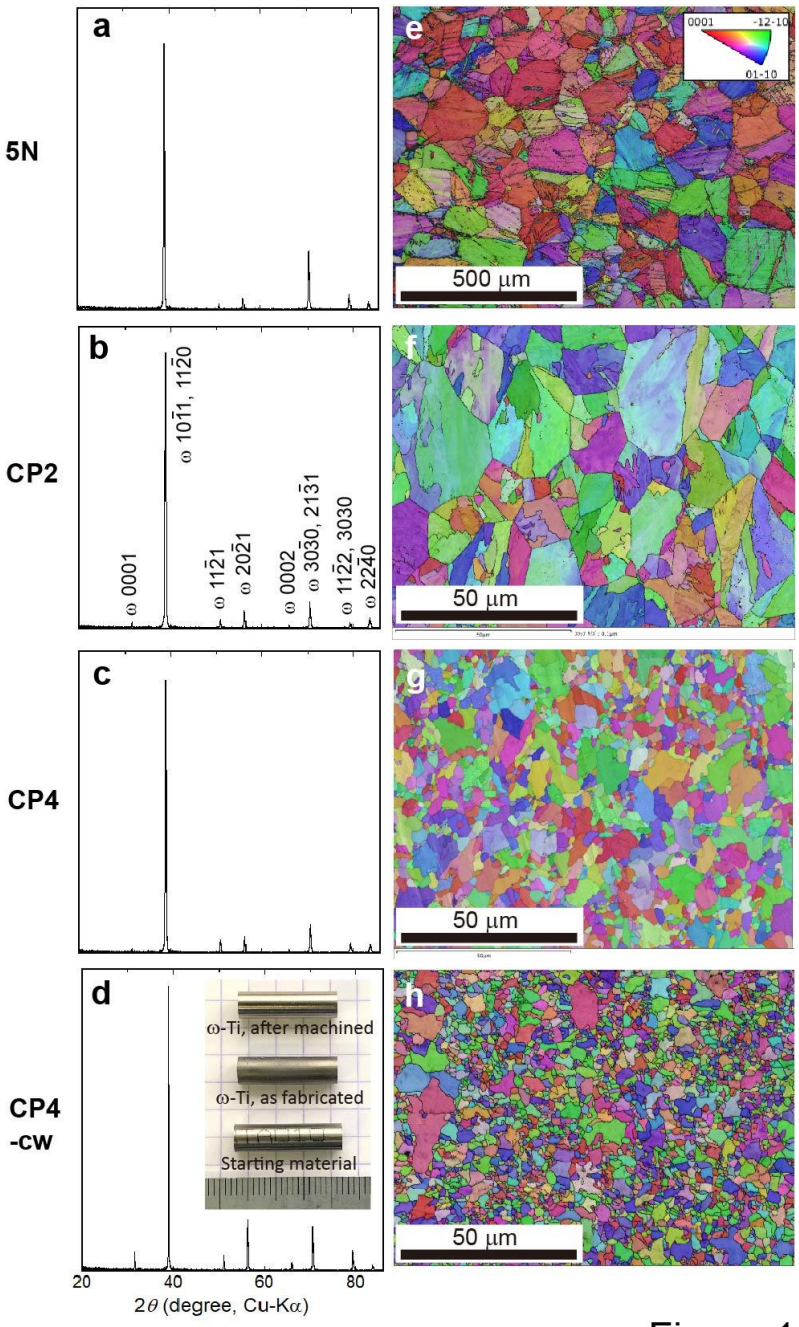

Figure 1. The characterization of polycrystalline ω-Ti materials with pure titanium compositions fabricated under high pressure and temperature conditions is presented. Four different starting materials (all α phase) were employed for the high-*PT* treatment: Ti 99.999 wt% metals basis (5N); CP-Ti Grade2 (CP2); CP-Ti Grade 4 (CP4); cold-worked CP-Ti Grade4 (CP4-cw). The X-ray diffraction patterns of the ω-Ti materials fabricated from 5N, CP2, CP4, and CP4-cw are shown in a) – d), respectively. It is evident that all the materials consist solely of the ω phase. The inset of d) presents a photograph of the titanium materials: the bottom, a starting material (CP4-cw); the middle, an ω-Ti material after high-*PT* treatment; the top, an ω-Ti material fabricated from CP4-cw after surface machining by a centerless grinder. The diameter of this object is 4.9 mm and its length is 17.7 mm. The samples were placed on a 5 mm grid paper. e) – h) were inverse pole figure (IPF) maps superimposed on band contrast (BC) images of the ω-Ti materials fabricated from 5N, CP2, CP4, and CP4-cw, respectively. The inset of e) shows the color coding for the orientations in e) – h). It is clear that grain size decreases from e) to h) (see text).

Figure 1

The mechanical properties of the ω-Ti materials were evaluated using miniature tensile test specimens. The specimens were prepared from the rod-shaped samples (see the inset in Fig 1d) using wire electrical discharge machining (EDM). After wire EDM cutting, a chemical polishing procedure was conducted using a commercially available liquid containing a nitric-hydrofluoric acid mixture to remove the damaged surface area[19]. After

chemical polishing, we conducted XRD measurements on the tensile specimens. The XRD profiles were essentially identical to those shown in Figures 1a-d, and the presence of a single phase of the ω phase in the tensile specimens was confirmed. As both the starting (α phase) and ω-Ti materials were tested, eight different stress-strain curves were obtained, and these curves are displayed in Figure 2. It is evident that, for each pure titanium composition, both the α-Ti and ω-Ti materials exhibited ductile behavior. We can also see that, for each composition, tensile strength of the ω-Ti material is greater than that of the α-Ti material. In addition, the impurity content exhibited a direct correlation with the yield strength and tensile strength of both the α and ω phases, with an increase observed from 5N to CP-Ti Grade 4 (see Figs. 2a-c). The impurity effect observed in the α-Ti material has been extensively documented in the literature[23,24] and is attributed to the presence of interstitial oxygen atoms[22-25], which have been shown to enhance the mechanical properties of the material. The present data indicate that the same strengthening mechanism is activated in the ω-Ti materials. Furthermore, as illustrated in Figures 2c and d, the strengths of the ω-Ti material increase with decreasing grain size (Figs. 1g and h). The strengthening of the α-Ti material in pure titanium due to grain size reduction is well documented[26] and is explained by the Hall-Petch effect[27,28]. The observed strengthening of the ω-Ti material can be attributed to this effect.

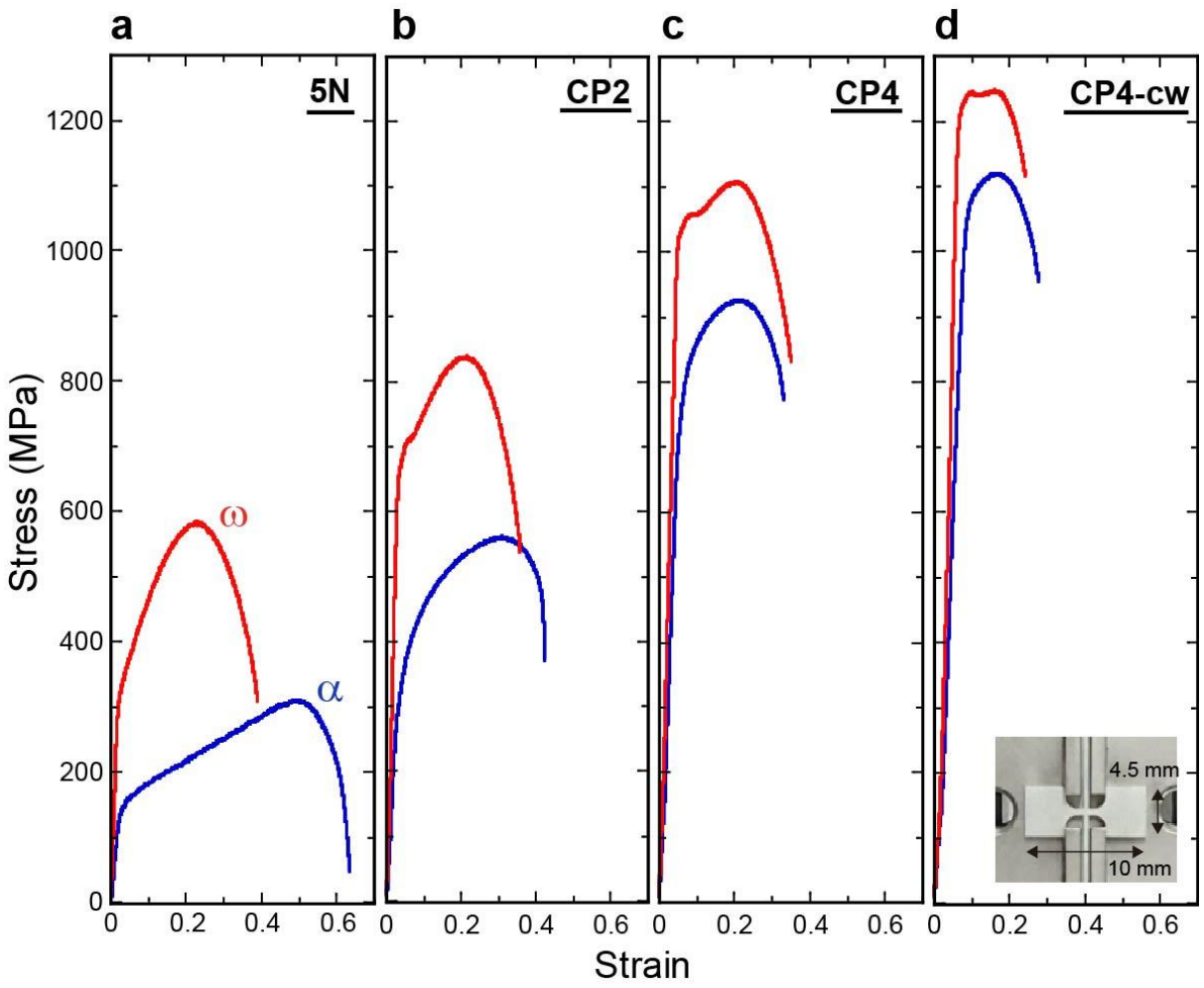

Figure 2

Figure 2. Stress-strain curves of the starting (α) and ω-Ti materials with pure titanium compositions obtained by miniature tensile tests. a) 5N (blue) and the ω-Ti material fabricated from 5N (red); b) CP2 (blue) and the ω-Ti material (red); c) CP4 (blue) and the ω-Ti material (red); d) CP4-cw (blue) and the ω-Ti material (red). The inset of d) shows a photograph of a miniature tensile specimen. In Fig. 2a, "α" refers to a stress-strain curve obtained from a bulk polycrystalline α-titanium material; "ω" refers to a stress-strain curve obtained from a bulk polycrystalline ω-titanium material (see text).

The 0.2% offset yield strength ($\sigma_{0.2\%}$), tensile strength (σ_{TS}), and elongation to failure (ε_f) were determined for all eight materials. The results are summarized in Table 1. For the ω-Ti material, which exhibited an average grain size of 3.4 ± 1.1 μm (Fig. 1h), fabricated from cold-worked CP-Ti grade 4, the following values were obtained. The yield strength, $\sigma_{0.2\%}$,

was determined to be 1130 ± 30 MPa, while the tensile strength, σ_{TS}, was found to be 1220 ± 30 MPa. The elongation to failure, ε_f, was measured to be 16 ± 2 %. The tensile strength and elongation to failure of this material are comparable to those of the most commonly used titanium alloy in industry, Ti-6Al-4V (Table 1 and Supplementary Figure 2). Figure 2 further illustrates that the ω-Ti materials demonstrate notable ductility, as exemplified by the elongation to failure of the ω-Ti material with CP-Ti grade 2 composition, which was determined to be 34 ± 1 %.

Table 1. Summary of mechanical properties of pure titanium materials determined by miniature tensile tests.

Phase	α				α+β	ω			
Material	5N	CP2	CP4	CP4-cw	Ti64	5N	CP2	CP4	CP4-cw
Grain size (μm)	-	-	-	-	-	65(16)	12(4)	5.2(17)	3.4(11)
$\sigma_{0.2\%}$ (MPa)	118(18)	257(15)	640(50)	973(5)	990(40)	264(9)	634(13)	990(20)	1130(30)
σ_{TS} (MPa)	284(11)	574(14)	930(20)	1121(7)	1190(70)	527(6)	833(11)	1090(30)	1220(30)
ε_f (%)	64(8)	40(2)	28(2)	22(1)	25(3)	38(2)	34(1)	30(2)	16(2)

The averages of the three tensile test runs for each material are shown with one standard deviation in parentheses.
Phase: a phase or phases that are present in the tensile specimens before starting the tensile tests.
5N: 99.999% Ti; CP2: CP-Ti Grade2; CP4: CP-Ti Grade4; CP4-cw; cold-worked CP-Ti Grade4; Ti64: Ti-6Al-4V.
$\sigma_{0.2\%}$: 0.2% offset yield strength; σ_{TS}: tensile strength; ε_f: elongation to failure.

In order to identify the phases present in a fractured specimen of the ω-Ti materials, a specimen with CP-Ti grade 2 composition was selected and X-ray diffraction (XRD) measurements were performed using transmission mode with high-energy synchrotron radiation. The XRD profiles were collected at 0.5 mm intervals along the tensile axis of the specimen. The value of *D* was defined based on the distance from the edge of grip section

toward the fracture surface (Fig. 3a). The fracture surface was positioned at D = 5.0 mm. The profiles collected at distances between D = 2.0 and 5.0 mm are displayed in Figure 3b. The XRD profiles collected at D = 2.0, 2.5, and 3.0 mm (from the grip section to the shoulder of the specimen) were found to be similar to those obtained prior to the tensile test (Fig. 1b). The XRD peaks of the ω phase were solely observed. At D = 3.5 mm, XRD peaks of the α phase appear and the intensity of these peaks increases with the distance D (4.0 and 4.5 mm). At the position including the fracture surface (D = 5.0 mm), XRD peaks of the ω phase disappear and those of the α phase are exclusively observed. It is noteworthy that the appearance of the α phase was also detected in fractured tensile specimens in other pure titanium compositions (Supplementary Figure 3). The XRD measurements of the fractured ω-Ti materials demonstrated that the ω→α transformation occurs in the gauge sections during the tensile tests. This observation indicates that the stress-strain curves of the ω-Ti materials are influenced by this transformation. It should therefore be noted that the values reported in Table 1 are not representative of those for the ω-phase itself.

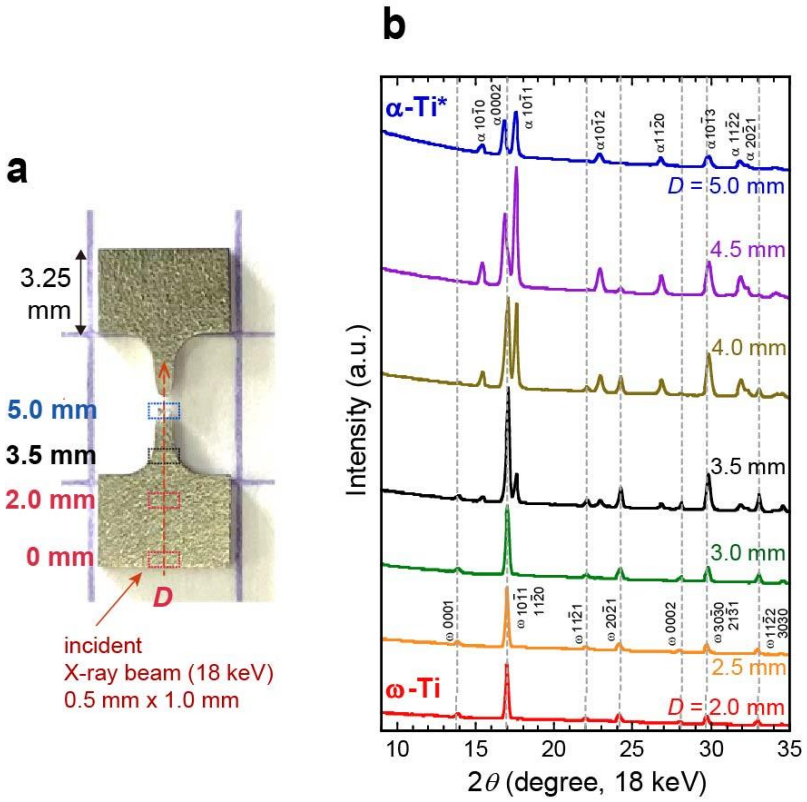

Figure 3. X-ray diffraction profiles obtained from a fractured ω-Ti tensile specimen. The ω-Ti material was fabricated from CP2. The fractured specimens were placed on a 5 mm grid paper. a) A photograph of fractured tensile specimens and definition of the distance from the edge of grip section, *D*. The beam size (1.0 mm × 0.5 mm) is shown by the dashed squares. b) X-ray diffraction profiles collected at different *D* positions from *D* = 2.0 mm (in the grip section) to *D* = 5.0 mm (the position including fracture surface). XRD peaks of the α phase can be seen in the gauge section between *D* = 3.5 and 5.0 mm.

Figure 3

An investigation into the microstructure of a fractured ω-Ti material (CP-Ti Grade2 composition) was conducted through the utilization of the FESEM-EBSD technique. As can be seen in Figure 4a, a cross section of the fractured tensile specimen was prepared. The observations were performed at four different positions where the α phase is present: *D* = 3.5, 4.0, 4.5 and 5.0 mm (Fig. 4b). Backscattered electron images (BEIs, Fig. 4c) demonstrate that grain size varies as a function of the distance *D*. At the position of *D* = 3.5 mm, the average grain size of the ω phase is comparable to that of an undeformed ω-Ti material (Fig. 1f). It is evident that the grain size decreases with the distance *D*. Furthermore, the presence of micropores near the fracture surface (*D* = 5.0 mm) was observed. These observations suggest

that plastic deformation leads to a reduction in grain size[29] and the formation of pores[30]. As can be seen from the band contrast (BC) images (Fig. 4d), the proportion of darker areas (i.e., weaker intensities of Kikuchi bands) increases with distance *D*. These observations suggest that plastic deformation leads to the formation of lattice defects[31]. The EBSD mappings were also used for phase analysis (Fig. 4e). At the position of D = 3.5 mm, the presence of small particles of the α phase was observed at grain boundaries of the ω phase. Moreover, at D = 4.0 mm, the presence of lamellar α phase was observed within the ω phase matrix. The proportion of the α phase increases at D = 4.5 mm and only the α phase was observed at the position including the fracture surface (D = 5.0 mm), which is consistent with the XRD data (Fig. 3b). These microstructure observations as well as the XRD data (Fig. 3) demonstrate that stress-induced ω → α transformation occurs during tensile deformation.

One of the unknown factors is the effect of hydrogen on the ω-Ti materials. In the present study, miniature tensile specimens were prepared using wire EDM cutting followed by chemical polishing. During these processes, hydrogen might be absorbed by the specimens, affecting their tensile behavior, including the stress-induced ω → α transformation. It is well known that hydrogen decreases the ductility and creep resistance of CP-Ti materials[32]. Future studies are needed to measure the hydrogen content of the ω-Ti materials and to examine the effect of hydrogen on the mechanical properties of these materials.

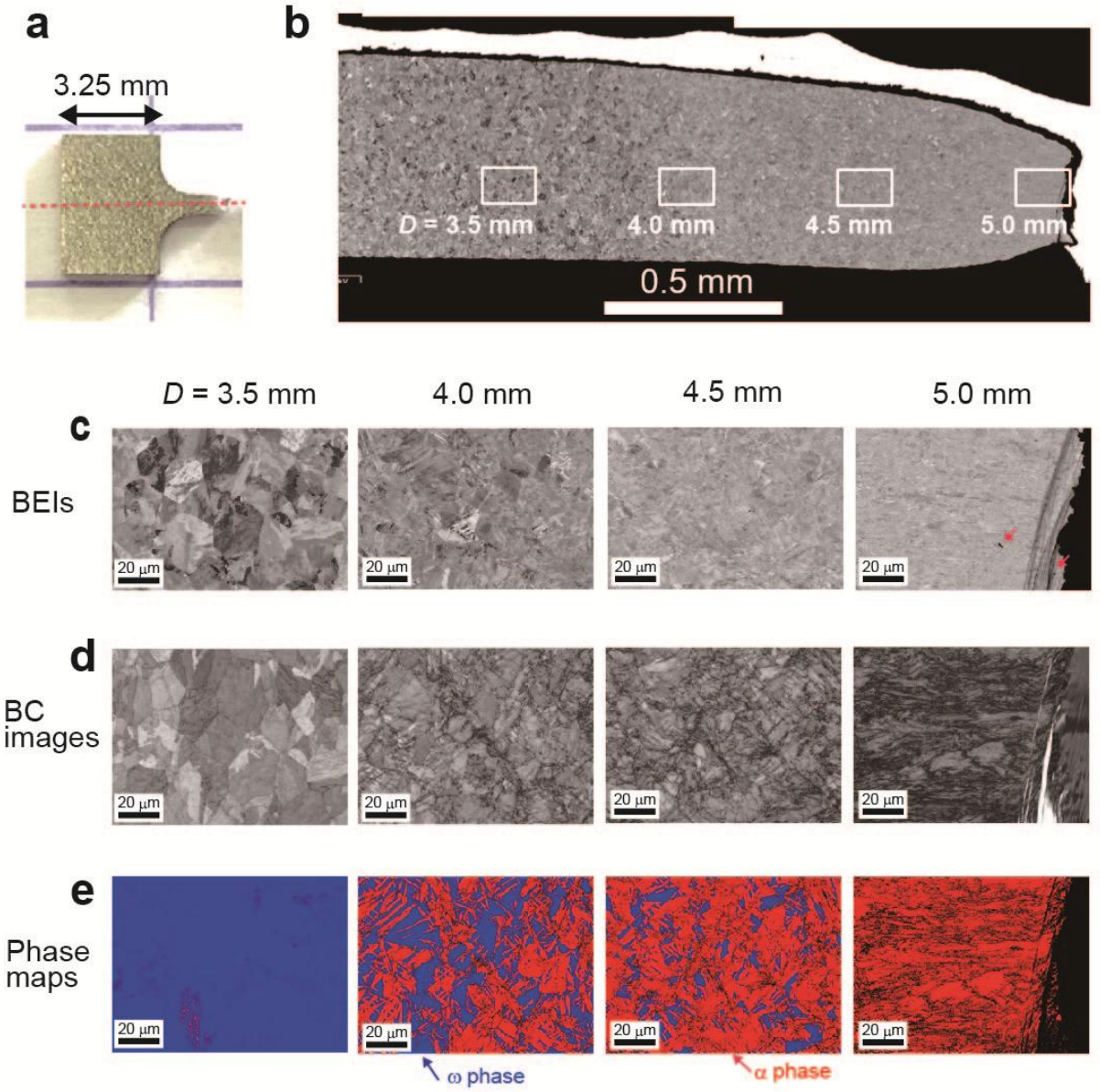

Figure 4

Figure 4. Microstructure observations of a fractured ω-Ti tensile specimen. The ω-Ti material was fabricated from CP2. a) Photograph of a fractured specimen. The dashed line indicates the position of the cross section for the observations. The cross section is perpendicular to the flat surface of the tensile specimen. b) Overview back-scattered electron image (BEI) of the investigated area. Detailed observations were conducted at positions where ω → α transformations occur: D = 3.5, 4.0, 4.5 and 5.0 mm. BEIs (c), band contrast (BC) images (d), and phase maps (e) are shown at these positions. In c), the red arrows indicate the locations of pores. At D = 4.0mm, the lamellar α phase was observed within the ω phase matrix.

It has been well established that martensitic α → ω transformation occurs in titanium[33-35]. The martensitic transformation induces two types of orientation relationships between the α and ω phases. They are referred to as Variant I (OR I) and Variant II (OR II) following Usikov and Zilbershtein's notation[33]:

OR I: $(0001)\alpha \parallel (01\bar{1}1)\omega$, $[11\bar{2}0]\alpha \parallel [\bar{1}011]\omega$,

ORII: $(0001)\alpha \parallel (11\bar{2}0)\omega$, $[11\bar{2}0]\alpha \parallel [0001]\omega$.

Given the fact that the ω phase is metastable at ambient conditions, the reverse process, ω → α transformation, has scarcely been studied. Zahili et al.[36] conducted molecular dynamics simulations and theoretically investigated the deformation process of ω-Ti. The authors predicted that the ω → α transformation also follows either OR I or OR II and demonstrated that OR I is energetically more favorable than OR II (the energy barrier of OR I is approximately one-quarter of that of OR II). In order to investigate the orientation relationships between the ω and α phases in fractured specimens obtained in the present study, more detailed microstructure analysis was performed using the FESEM-EBSD technique. The specimen observed in Figure 4 was analyzed.

Observations were conducted at a position of D = 3.75 mm, where the area fraction of the α-phase is less than that at D =3.5 mm (see Fig. 4e). The presence of thin lamellar α-phase is clearly observable within ω grains (Fig. 5a). Figures 5b, c, and d represent EBSD inverse pole figure maps of ω-phase, α-phase, and both phases, respectively. In each ω grain with the

lamellar texture, the thin layered α grains that are arranged parallel to each other appear to be oriented to the same crystallographic orientation. This result strongly indicates the presence of an orientation relationship between the original ω phase and the resultant α phase. Figure 5e represents an EBSD grain boundary map at the same position. Grain boundaries between two grains with the same crystal structure (i.e., ω/ω and α/α grain boundaries) are represented by black lines, whereas those between two different phases (i.e., ω/a grain boundaries) are represented by colored lines. The red and blue grain boundaries satisfy the orientation relationships, OR I and OR II, respectively. It has been demonstrated that the majority of the long and straight ω/α boundaries are explained by OR I, and that the OR II grain boundaries are significantly shorter than those of OR I. Utilizing this image, the boundary line lengths (BLLs) of these three types of grain boundaries were calculated. In the specific position (D = 3.75 mm), characterized by an area fraction of 11% for the α-phase, the OR I grain boundary occupies 73% of the total ω/α phase boundary. In contrast, the OR II grain boundary only occupies 11%. This phenomenon can be attributed to the energetic favorability of OR I (ref. 35). The same grain-boundary analysis was subsequently conducted at other locations within the fractured specimen: D = 4.0, 4.5 and 4.65 mm (Figs. 5f, g, and h). The results are summarized in Figure 5i. It has been demonstrated that the ratio of OR I grain boundary decreases with D, while the ratio of OR II grain boundary increases slightly with D. Since the OR I grain boundary is primarily observable in relatively larger ω grains (Fig. 5a),

this tendency with *D* (i.e., the distance from the edge of grip section toward the fracture surface along the tensile axis, see Fig. 3a) may be associated with the increase of α-phase fraction (i.e., the decrease of ω-phase fraction) and the grain size reduction observed in Figure 4. Moreover, transmission electron microscope (TEM) observations were performed on the fractured specimen. The presence of an orientation relationship that is identical to OR I was also observed between the ω and α phases (Supplementary Figure 5). The data obtained by FESEM-EBSD and TEM demonstrate that stress-induced ω → α martensitic transformation occurs during tensile deformation.

Further TEM studies, especially high-resolution observations, are needed to elucidate the phase transformation process from the ω to α phase under deformation. Figure 5a clearly shows the presence of thin α-phase layers in ω grains. During the initial stage of deformation, α-phase nucleation may occur on a nanoscale at the grain boundaries of ω grains and/or within ω-phase grains. Understanding the phase transformation process can be beneficial to controlling the mechanical properties of the ω-Ti materials.

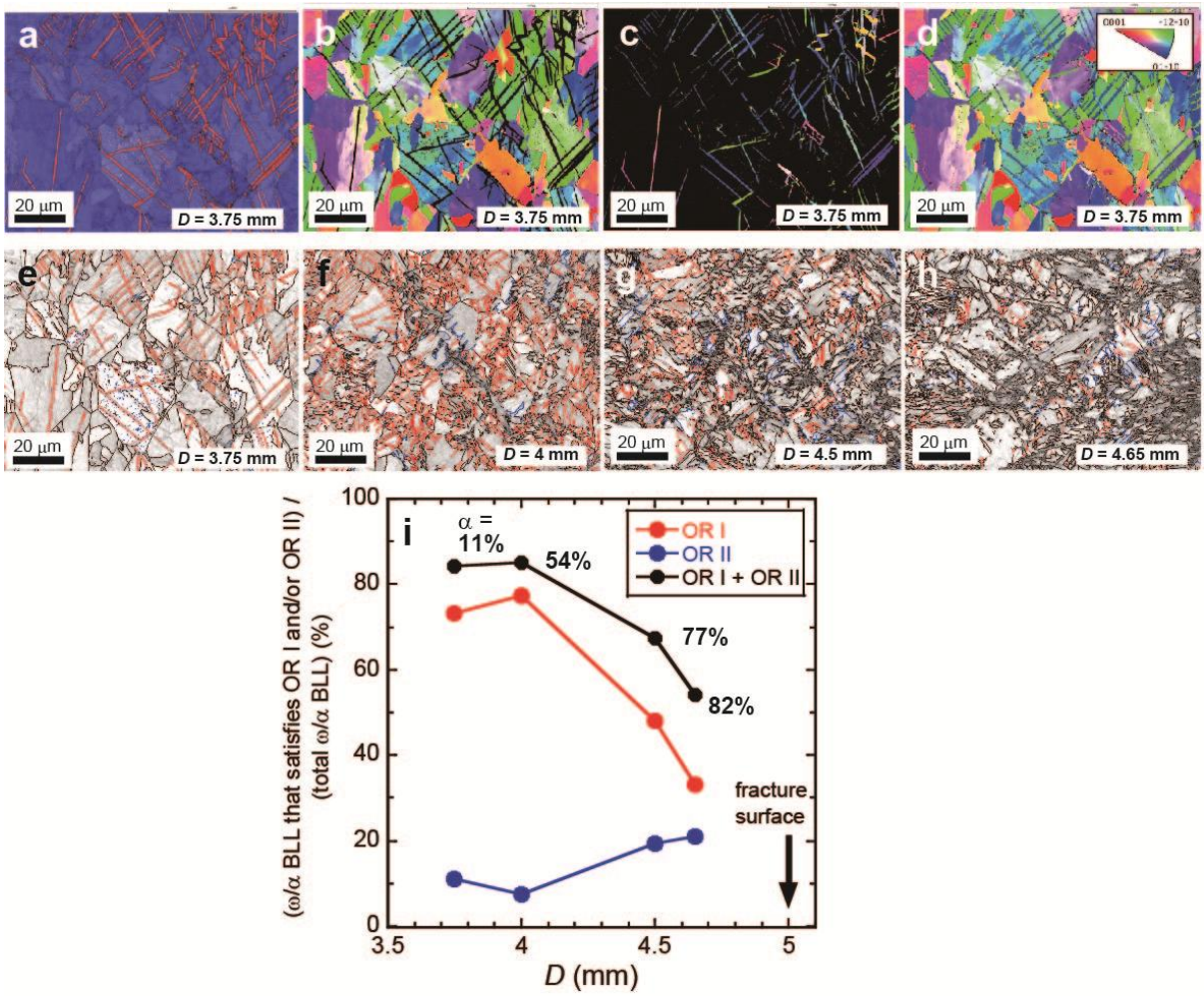

Figure 5

Figure 5. Crystal orientation maps by EBSD at a position of D = 3.75 mm (a-d) and grain boundary maps at different positions (e-h) within the fractured ω-Ti tensile specimen. a) A phase map illustrating the distribution of the α and ω phases at a position of D = 3.75 mm. The presence of thin lamellar α-phase is clearly observable within ω grains. b-d) Inverse pole figure maps of ω, α, and both phases at a position of D =3.75 mm, respectively. e-h) Grain boundary maps at D = 3.75, 4.0, 4.5, and 4.65 mm, respectively. The grain boundaries between the ω and α phases are represented by colored lines. The red and blue lines represent the grain boundaries that satisfy the orientation relationships, OR I and OR II, respectively. i) The ratios of ω/α boundary line length (BLL) that satisfy the orientation relationship of OR I at different D positions are represented by red symbols. The ratios of ω/α BLL that satisfy OR II at different D positions are represented by blue symbols. The former exhibits a decrease, while the latter displays a slight increase with D.

In order to investigate the process of this stress-induced transformation, time-resolved synchrotron XRD measurements of the ω-Ti material with CP-Ti Grade 2 composition were conducted during a tensile test. Figure 6 summarizes the results obtained from the

measurements. A miniature tensile specimen was mounted on a portable mechanical testing device and pulled to failure at a constant cross-head displacement rate (0.5 μm/s). XRD profiles were collected at 2-second intervals, and the complete set of profiles obtained until failure are shown in Figure 6a. The initial profile, which indicates the presence of a single phase ω, is depicted in Figure 6b. The final profile, recorded just before the failure of the tensile specimen, depicts the coexistence of the α and ω phases (Fig. 6c). The relationship between nominal stress and elapsed time (t) is illustrated in Figure 6d. Since the crosshead speed is constant, this diagram corresponds to a nominal stress-strain curve of the ω-Ti material. It is evident that the specimen undergoes elastic deformation up to $t \sim 500$ s, and no transformation to the α phase occurs in the elastic regime. At $t \sim 600$ s, the XRD peaks of the α phase appeared, and the peak intensities increased with increasing elapsed time. The volume fraction of the α phase was calculated using the XRD data with the reference intensity ratio (RIR) method. The results are shown in Figure 6e. It is observed that, following the appearance of the α phase, the volume fraction undergoes a rapid increase up to $t \sim 900$ s within the region of uniform plastic deformation (Fig. 6d). Subsequent to reaching the ultimate tensile strength ($t \sim 1100$ s), the volume fraction remains constant at approximately 65% until fracture. As demonstrated in Figures 3b and 4e, the ω phase undergoes complete transformation into the α phase at the fracture position. This discrepancy can be attributed to the misalignment between the X-ray beam position on the tensile

specimen and the fracture position. The data presented in Figures 3-6 demonstrate that stress-induced ω → α martensitic phase transformation occurs exclusively in the plastic regime. The present study revealed transformation-induced plasticity[37] (TRIP) in the ω-Ti materials.

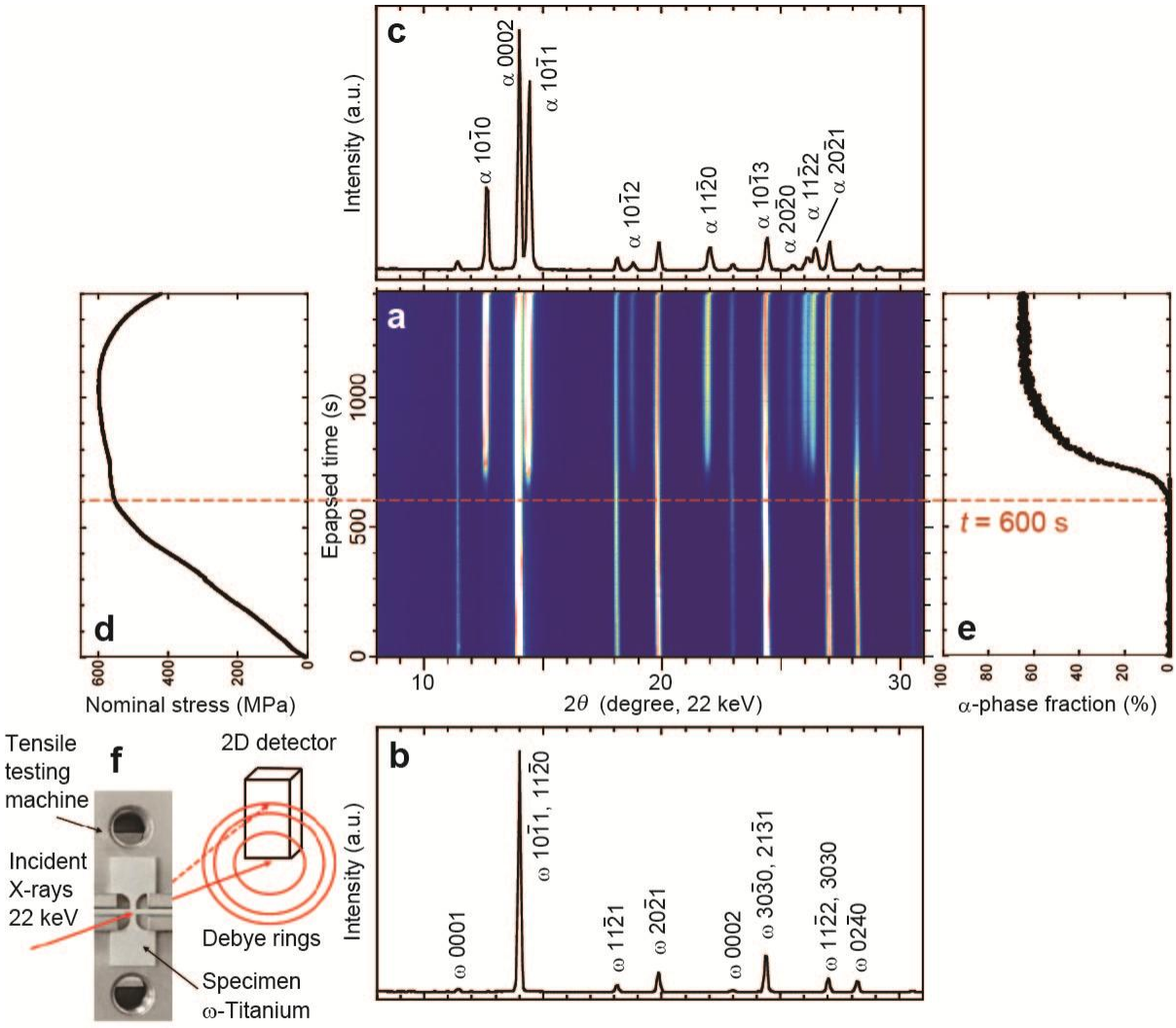

Figure 6

Figure 6. Results of time-resolved synchrotron XRD measurements of an ω-Ti material during a tensile test. The ω-Ti material was fabricated from CP2. a) All the XRD profiles obtained by the time-resolved data collection (every 2 s). The color contrast represents peak intensity. b) The profile recorded immediately after the crosshead was moved. c) The profile recorded instantly prior to the failure of the tensile specimen. d) Nominal stress versus elapsed time plot. This corresponds to the nominal stress-stain curve because the crosshead speed is constant (0.5 μm/s). e) Calculated volume fraction of the α phase as a function of elapsed time. The stress-induced ω → α transformation proceeds in the plastic regime. f) A schematic illustration of the experimental

The tensile behavior of the ω-Ti materials may be explained by that of the mixture of the ω and α phases. However, it should be noted that, as the plastic deformation proceeds, the volume fraction of the α-phase increases (Fig. 6a) and grain sizes of the both phases decrease (Figs. 4 and 5). Moreover, measuring the mechanical properties of the ω-phase itself under ambient conditions poses a substantial challenge, owing to the inherent thermodynamic metastability. Tensile testing at cryogenic temperatures may be advantageous in observing the tensile behavior of the ω-phase, as it can suppress the ω → α phase transformation[1].

The results of the present experimental study are consistent with those of previous theoretical studies. Zong et al.[38] conducted molecular dynamics (MD) simulations in pristine single crystal ω-titanium. They found a highly anisotropic deformation behavior, brittle fracture and superplastic deformation depending on the crystallographic orientation. In a subsequent study, Zahiri et al.[36] performed large-scale MD simulations in the ω phase with initial defects, which are inevitably contained in real titanium materials, particularly in the ω-phase. The authors found that stress-induced ω → α martensitic transformation causes extensive plasticity under various loading directions with respect to the crystallographic orientation. The findings of these studies[36,38] demonstrated that the ω phase undergoes elastic deformation at the initial stage of deformation and that the ω → α martensitic transformation occurs exclusively within the plastic regime. In the present experimental study, the majority of the theoretically predicted phenomena that occur during deformation of ω-Ti were

successfully observed. A notable absence from the present study was the observation of phase transformation sequence from ω to α phase. Zahiri et al[36] predicted that the ω → α phase transformation following OR I invariably involves a thin layer of the β-phase at the ω/α interface. Further TEM observations are necessary to elucidate the nature of this transformation sequence.

CP-Ti and Ti-6Al-4V are frequently utilized in biomedical applications due to their exceptional corrosion resistance[39]. However, it should be noted that both materials possess certain limitations[40]. CP-Ti exhibits comparatively lower mechanical strength, while Ti-6Al-4V has the potential to induce toxicity through the release of ions (Al and V). Since the 1960s, CP-Ti has been the preferred material for dental implant devices to prevent cytotoxicity[41]. The present study demonstrates that the ω-Ti material with CP-Ti Grade 4 composition exhibits equivalent strength to that of Ti-6Al-4V (Table 1). This finding indicates that the ω phase in pure titanium may have potential applications as a biomaterial, for instance in dental and spinal implants. The role of passive film on titanium and its alloys is crucial for their excellent biocompatibility[42]. Therefore, investigation of the passive film on the ω-Ti materials may be beneficial for the evaluation of the biocompatibility.

Methods

Synthesis under high-pressure and temperature. High pressure and high temperature synthesis runs were conducted using Kawai-type apparatus[43], with tungsten carbide cubes serving as the second stage anvils. The pressure transmitting medium was octahedral-shaped semi-sintered magnesia doped with Cr_2O_3. A cylindrical graphite furnace was employed, with a sample container made of hBN and MgO embedded into the furnace. The initial compression of the sample was conducted at pressures ranging from 9 to 12 GPa at ambient temperature. Subsequently, the temperature was elevated to a range of 400 to 500˚C. The grain size of the ω-Ti materials was controlled through the implementation of various time-temperature profiles. Further details can be found in the supplementary information.

XRD measurements and microstructure observations of ω-Ti materials. The rod-shaped ω-Ti materials after high-*PT* treatment (see inset of Fig.1d) were chemically polished using a commercially available liquid containing a nitric hydrofluoric acid mixture[19]. XRD measurements on the flat surfaces of the rod-shaped specimens were performed by the reflection geometry using a benchtop X-ray diffractometer (Miniflex600, Rigaku, Tokyo, Japan) with Cu anode. For each ω-Ti material, a cross-section parallel to the rod-axis was prepared and chemically polished to observe the microstructure. We used a FESEM (Gemini450, Zeiss AG, Germany) equipped with an EBSD detector (Symmetry, Oxford

Instruments, UK). Typical operating parameters were 15 keV accelerating voltage and 10 nA beam current. The step size utilized for the EBSD analysis was set at 100 nm.

Miniature tensile tests. Tensile specimens were extracted from the rod-shaped ω-Ti materials (inset of Fig. 1d) through the implementation of wire EDM. The tensile axis of the specimen is parallel to the rod axis. The fabrication process commonly yielded two specimens from a single rod. After wire EDM cutting, the specimens underwent a chemical polishing procedure to remove the damaged surface layer[19]. The total length and width of the specimen are 10 and 4.5 mm, respectively (Fig. 2d). The gauge length and gauge section are 1.5 mm and 0.7 × 0.7 mm^2, respectively. Each tensile specimen was mounted horizontally on grips and pulled to failure using a testing machine[44] operating at a constant rate of cross-head displacement. The initial strain rate of each test was 5.5×10^{-4} s^{-1}. The stress and strain of the specimens were calculated by utilizing the applied load and cross-head displacement, respectively, on the assumption that the gauge section deforms uniformly and that its volume is constant throughout the tensile tests. It is noteworthy that, in the present study, all the tensile tests were conducted under identical testing conditions, thereby ensuring internal consistency. It is also important to note that the present tensile specimens are relatively small. Therefore, when comparing the present data with other results obtained by using tensile specimens with different dimensions, caution should be taken[45,46]. Nevertheless, it should be noted that the

tensile strength and elongation to failure of Ti-6Al-4V determined in the present study (Table 1 and Supplementary Fig. 2) are reasonably consistent with those reported in a previous study conducted by using larger tensile specimens[47].

High energy XRD measurements for fractured specimens. The measurements were conducted at BL16, SAGA Light Source, Japan. Synchrotron X-rays from a 4T superconducting wiggler were monochromatized by a Si (111) double-crystal monochromator. The higher harmonics were subsequently removed by utilizing a Pt-coated mirror. The X-ray energy of the incident beam was 18 keV. The X-rays were then collimated by slits into beams with a width of 1.0 mm and a height of 0.5 mm, which were irradiated on the specimens. The diffracted X-rays were recorded by a 2D detector (Pilatus 100K-S, Dectris AG, Switzerland). The X-ray energy and the sample-to-detector distance (152.5 mm) were calibrated using a CeO_2 standard (NIST SRM 674a). The typical exposure time was 10 seconds.

Microstructure observations for a fractured specimen. A fractured specimen was mounted in epoxy resin and ground to expose a cross section parallel to the tensile axis and perpendicular to the flat surface of the tensile specimen (Fig. 4a). The cross section was then subjected to a polishing procedure using an Ar ion beam (IB-09020CP, JEOL Ltd., Japan).

The microstructure was then examined by utilizing the FESEM-EBSD technique. The instruments and operating parameters were identical to those employed for the ω-Ti materials.

Time-resolved XRD measurements during a tensile test. The measurements were conducted at BL16, SAGA Light Source, Japan. The X-ray energy of the incident beam was 22 keV. The X-rays were collimated by slits into 0.3 mm in width and 0.5 mm in height and irradiated on the gauge section of the tensile specimen. A portable tensile testing device (TST350, Linkam Scientific Instruments Ltd., UK) was employed, which is mounted on motorized two-axis (perpendicular to the X-ray beam) translation stages to adjust the sample position[48]. The experimental setup for the XRD measurements is similar to that for fractured specimens, with the sample-to-detector distance set at 175.6 mm.

Data availability

The data that support the findings of this study are available from the corresponding author upon reasonable request.

References

1. Hennig, R. G., Lenosky, T. J., Trinkle, D. R., Rudin, S. P. & Wilkins J. W. Classical potential describes martensitic phase transformations between α, β, and ω titanium phases. *Phys. Rev. B* **78**, 054121 (2008).
2. Jamieson, J. C. Crystal structures of titanium, zirconium, and hafnium at high pressures. Science **140**, 72-73 (1963).
3. Akahama, Y., Kawamura, H., & Le Bihan, T. New δ (Distorted-bcc) Titanium to 220 GPa. *Phys. Rev. Lett.* **87**, 275503 (2001).
4. Dewaele, A., Stutzmann, V., Bouchet, J., Bottin, F., Occelli, F., & Mezouar, M. High pressure-temperature phase diagram and equation of state of titanium. *Phys. Rev. B* **91**, 134108 (2015).
5. Ankem, S. & Greene, C. A. Recent developments in microstructure/property relationships of beta titanium alloys. *Mater. Sci. Eng. A* **263**, 127-131 (1999).
6. Mohammed, M. T., Khan, Z. A. & Siddiquee, A. N. Beta titanium alloys: the lowest elastic modulus for biomedical applications: a review. *Int. J. Chem. Nucle. Metall. Mater. Eng.* **8**, 726-731 (2014).
7. Hickman, B. S. The formation of omega phase in titanium and zirconium alloys: a review. *J. Mater. Sci.* **4**, 554-563 (1969).
8. Williams, J. C., Hickman, B. S., & Marcus, H. L. The effect of omega phase on the mechanical properties of titanium alloys. *Metall. Trans.* **2**, 1913-1919 (1971).

9. Sun, F. et al. Strengthening strategy for a ductile metastable β-titanium alloy using low-temperature aging. *Mater. Res. Lett.* **5**, 547-553 (2017).

10. Koul, M. K. & Breedis, J. F. Omega phase embrittlement in aged Ti-V. *Metall. Trans.* **1**, 1451-1452 (1970).

11. Brumbauer, F., Okamoto, N. L., Ichitsubo, T., Sprengel, W. & Luckabauer, M. Minor additions of Sn suppress the omega phase formation in beta titanium alloys. *Acta Mater.* **262**, 119466 (2024).

12. Illarionov, A. G., Popov, A. A., Grib, S. V. & Elkina, O. A. Special features of formation of omega-phase in titanium alloys due to hardening. *Metal Sci. Heat Treat.* **52**, 493-498 (2011).

13. Sun, F. et al. Strengthening strategy for a ductile metastable β-titanium alloy using low-temperature aging. *Mater. Res. Lett.* **5**, 547-553 (2017).

14. Quin, B. et al. Mechanisms underlying enhanced strength-ductility combinations in TRIP/TWIP Ti-12Mo alloy engineered via isothermal omega precipitation. *Acta Mater.* **245**, 118619 (2023).

15. Todaka, Y., Sasaki, J., Moto, T. & Umemoto, M. Bulk submicrocrystalline ω-Ti produced by high-pressure torsion straining. *Scripta Mater.* **59**, 615-618 (2008).

16. Tane, M., Okuda, Y., Todaka, Y., Ogi, H. & Nagakubo, A. Elastic properties of single-crystalline ω phase in titanium. *Acta Mater.* **61**, 7543-7554 (2013).

17. Trinkle D. R. et al. Empirical tight-binding model for titanium phase transformations. *Phys. Rev. B* **73**, 094123 (2006).

18. Li, S., Yuan, Q., Zhang J., Li, Y. & He, D. Towards pure: The single-phase bulk omega titanium and modulation on its elastic properties under biaxial strains. *J. Alloys Compd.* **906**, 164312 (2022).

19. Sawahata, T. et al. High compressive strength of bulk polycrystalline ω phase in pure titanium. *Mater. Trans.* **66**, 616-621 (2025).

20. Vohra, Y. K., Sikka, S. K., Vaidya, S. N. & Chidambaram, R. Impurity effects and reaction kinetics of the pressure-induced α → ω transformation in Ti. *J. Phys. Chem. Solids* **38**, 1293-1296 (1977).

21. Cerreta, E., Gray III, G. T., Lawson, A. C., Mason, T. A. & Morris, C. E. The influence of oxygen content on the α to ω phase transformation and shock hardening of titanium. *J. Appl. Phys.* **100**, 013530 (2006).

22. Hennig, R. G. et al. Impurities block the α to ω martensitic transformation in titanium. *Nat. Mater.* **4**, 129-133 (2005).

23. Finlay, W. L. & Snyder, J. A. Effect of three interstitial solutions (nitrogen, oxygen, and carbon) on the mechanical properties of high-purity, alpha titanium. *JOM* **2**, 277-286 (1950)

24. Simbi, D. J. & Scully, J. C. The effect of residual interstitial elements and iron on mechanical properties of commercially pure titanium. *Mater. Lett.* **26**, 35-39 (1996).

25. Oh, J. M. et al. Oxygen effects on the mechanical properties and lattice strain of Ti and Ti-6Al-4V. *Met. Mater. Int.* **17**, 733-736 (2011).

26. Miura, H., Kobayashi, M., Aoba, T., Aoyama, H. & Benjanarasuth, T. An approach for room-temperature multi-directional forging of pure titanium for strengthening. *Mater. Sci. Eng. A* **731**, 603-608 (2018).

27. Hall, E. O. The deformation and ageing of mild streel: III discussion of results. *Proc. Phys. Soc. Lond.* **64**, 747-753 (1951).

28. Petch, N. J. The cleavage strength of polycrystals. *J. Iron Steel Inst.* **173**, 25-28 (1953).

29. Li, X. & Lu, K. Refining grains of metals through plastic deformation: toward grain size limits. *Acc. Mater. Res.* **2**, 108-113 (2021).

30. Rusinko, A. K., Ginsztler, J. & Devenyi, L. Analytic description of the formation of pores under conditions of steady-state creep of metals. *Strength Mater.* **39**, 74-79 (2007).

31. Van Bueren, H. G. Theory of the formation of lattice defects during plastic deformation. *Acta Metall*. **3**, 519-524 (1955).

32. Wasz, M. L., Brotzen, F. R., McLellan, R. B., Griffin, A. J. Effect of oxygen and hydrogen on mechanical properties of commercial purity titanium. *Inter. Mater. Rev.* **41**, No.1 (1996).

33. Usikov, M. P. & Zilbershtein, V. A. The orientation relationship bwtween the w-phases of titanium and zirconium. *Phys. Status Solidi A* **19**, 53-58 (1973).

34. Trinkle, D. et al. New mechanism for the α to ω martensitic transformation in pure titanium. *Phys. Rev. Lett.* **91**, 025701 (2003).

35. Silcock, J. M. An x-ray examination of the ω phase in TiV, TiMo and TiCr alloys. *Acta Metallur.* **6**, 481-493 (1958).

36. Zahiri, A. H., Ombogo, J., Ma, T., Chakraborty, P. & Cao L. Transformation-induced plasticity in omega titanium. *J. Appl. Phys.* **129**, 015105 (2021).

37. Fischer, F. D. et al. A new view on transformation induced plasticity (TRIP). *Int. J. Plast.* **16**, 723-748 (2000).

38. Zong, H., Xue, D., Ding, X. & Lookman, T. Phase transformations in titanium: anisotropic deformation of ω phase. *J. Phys.: Conf. Ser.* **500**, 112042 (2014).

39. Shah, F. A., Trobos, M., Thomsen, P. & Palmquist, A. Commercially pure titanium (cp-Ti) versus titanium alloy (Ti6Al4V) materials as bone anchored implants – is one truly better than the other? *Mater. Sci. Eng. C* **62**, 960-966 (2016).

40. Nicholson, J. W. Titanium alloys for dental implants: a review. *Prosthesis* **2**, 100-116 (2020).

41. Buser, D., Sennerby, L. & De Bruyn, H. Modern implant dentistry based on osseointegration: 50 years of progress, current trends and open questions. *Periodontology 2000*, **73**, 7-21 (2017).

42. Hanawa, T. Biocompatibility of titanium from the viewpoint of its surface. *Sci. Tech. Adv. Mater.* **23**, 457-472 (2022).

43. Kawai, N. & Endo, S. The generation of ultrahigh hydrostatic pressures by a split sphere apparatus. *Rev. Sci. Instrum.* **41**, 1178-1181 (1970).

44. Horita, Z. & Langdon, T. G. Achieving exceptional superplasticity in a bulk aluminum alloy processed by high-pressure torsion. *Scripta Mater.* **58**, 1029-1032 (2008).

45. Edalati, K., Matsubara, E. & Horita Z. Processing pure Ti by high-pressure torsion in wide ranges of pressures and strain. *Metall. Mater. Trans. A* **40A**, 2079-2086 (2009).

46. Zhao, Y. H. Influence of specimen dimensions on the tensile behavior of ultrafine-grained Cu. *Scripta Mater.* **59**, 627-630 (2008).

47. Hu, H., Xu, Z., Dou, W. & Huang, F. Effect of strain rate and stress state on mechanical properties of Ti-6Al-4V alloy. Int. J. Impact Eng. 145, 103689 (2020).

48. Tokuda, K., Goto, K., Iihara, J. & Adachi, H. Visualization of local deformation in metallic materials through in situ X-ray diffraction mapping. *Mater. Trans.* **66**, 50-55 (2025).

Acknowledgements

We thank T. Hanawa, H. Hosoda, A. Holtzheid, T. Nakano, P. Wiedekehr, M. Pawelkiewicz-Koebel, H. Fujii, and M. Goto for discussion. We also thank H. Ichihara, K. Manabe, I. Sou, J. Li, H. Muto, and H. Ikeda for technical assistance. Synchrotron XRD measurements were conducted at BL16, SAGA-LS (project number: SEI2023C-012, SEI2024B-012). This research was supported by Japan Society for the Promotion of Science, a Grant-in-Aid for Scientific Research on the innovation area “Science of New-Class of Materials Based on Elemental Multiplicity and Heterogeneity (Grant No. 18H05452)” partially to N.N.

Funding

Open access funding provided by Sumitomo Electric Industries, Ltd.

Author Contributions

N.N., K.S., F.W., and Z.H. designed the research. N.N., M.M., Y.K., A.F., and Z.H. led the project. N.N., Y.T., and T.Sawahata performed high-pressure synthesis. Y.T. and T.Sawahata performed XRD measurements. Y.T., T.Sawahata, and Z.H. performed tensile tests. K. Tominaga and T.Sekiya performed FESEM-EBSD measurements. K.K. performed TEM observations. N.N. and K.Tokuda performed synchrotron XRD measurements. N.N., M.M., and Z.H. wrote the manuscript with contributions from other authors.

Figure 1. The characterization of polycrystalline ω-Ti materials with pure titanium compositions fabricated under high pressure and temperature conditions is presented. Four different starting materials (all α phase) were employed for the high-*PT* treatment: Ti 99.999 wt% metals basis (5N); CP-Ti Grade2 (CP2); CP-Ti Grade 4 (CP4); cold-worked CP-Ti Grade4 (CP4-cw). The X-ray diffraction patterns of the ω-Ti materials fabricated from 5N, CP2, CP4, and CP4-cw are shown in a) – d), respectively. It is evident that all the materials consist solely of the ω phase. The inset of d) presents a photograph of the titanium materials: the bottom, a starting material (CP4-cw); the middle, an ω-Ti material after high-*PT* treatment; the top, an ω-Ti material fabricated from CP4-cw after surface machining by a centerless grinder. The diameter of this object is 4.9 mm and its length is 17.7 mm. The samples were placed on a 5 mm grid paper. e) – h) were inverse pole figure (IPF) maps superimposed on band contrast (BC) images of the ω-Ti materials fabricated from 5N, CP2, CP4, and CP4-cw, respectively. The inset of e) shows the color coding for the orientations in e) – h). It is clear that grain size decreases from e) to h) (see text).

Figure 2. Stress-strain curves of the starting (α) and ω-Ti materials with pure titanium compositions obtained by miniature tensile tests. a) 5N (blue) and the ω-Ti material fabricated from 5N (red); b) CP2 (blue) and the ω-Ti material (red); c) CP4 (blue) and the ω-Ti material (red); d) CP4-cw (blue) and the ω-Ti material (red). The inset of d) shows a

photograph of a miniature tensile specimen. In Fig. 2a, "α" refers to a stress-strain curve obtained from a bulk polycrystalline α-titanium material; "ω" refers to a stress-strain curve obtained from a bulk polycrystalline ω-titanium material (see text).

Figure 3. X-ray diffraction profiles obtained from a fractured ω-Ti tensile specimen. The ω-Ti material was fabricated from CP2. The fractured specimens were placed on a 5 mm grid paper. a) A photograph of fractured tensile specimens and definition of the distance from the edge of grip section, *D*. The beam size (1.0 mm × 0.5 mm) is shown by the dashed squares. b) X-ray diffraction profiles collected at different *D* positions from *D* = 2.0 mm (in the grip section) to *D* = 5.0 mm (the position including fracture surface). XRD peaks of the α phase can be seen in the gauge section between *D* = 3.5 and 5.0 mm.

Figure 4. Microstructure observations of a fractured ω-Ti tensile specimen. The ω-Ti material was fabricated from CP2. a) Photograph of a fractured specimen. The dashed line indicates the position of the cross section for the observations. The cross section is perpendicular to the flat surface of the tensile specimen. b) Overview back-scattered electron image (BEI) of the investigated area. Detailed observations were conducted at positions where ω → α transformations occur: *D* = 3.5, 4.0, 4.5 and 5.0 mm. BEIs (c), band contrast (BC) images (d), and phase maps (e) are shown at these positions. In c), the red arrows

indicate the locations of pores. At D = 4.0mm, the lamellar α phase was observed within the ω phase matrix.

Figure 5. Crystal orientation maps by EBSD at a position of D = 3.75 mm (a-d) and grain boundary maps at different positions (e-h) within the fractured ω-Ti tensile specimen. a) A phase map illustrating the distribution of the α and ω phases at a position of D = 3.75 mm. The presence of thin lamellar α-phase is clearly observable within ω grains. b-d) Inverse pole figure maps of ω, α, and both phases at a position of D =3.75 mm, respectively. e-h) Grain boundary maps at D = 3.75, 4.0, 4.5, and 4.65 mm, respectively. The grain boundaries between the ω and α phases are represented by colored lines. The red and blue lines represent the grain boundaries that satisfy the orientation relationships, OR I and OR II, respectively. i) The ratios of ω/α boundary line length (BLL) that satisfy the orientation relationship of OR I at different D positions are represented by red symbols. The ratios of ω/α BLL that satisfy OR II at different D positions are represented by blue symbols. The former exhibits a decrease, while the latter displays a slight increase with D.

Figure 6. Results of time-resolved synchrotron XRD measurements of an ω-Ti material during a tensile test. The ω-Ti material was fabricated from CP2. a) All the XRD profiles obtained by the time-resolved data collection (every 2 s). The color contrast represents peak

intensity. b) The profile recorded immediately after the crosshead was moved. c) The profile recorded instantly prior to the failure of the tensile specimen. d) Nominal stress versus elapsed time plot. This corresponds to the nominal stress-stain curve because the crosshead speed is constant (0.5 μm/s). e) Calculated volume fraction of the α phase as a function of elapsed time. The stress-induced ω → α transformation proceeds in the plastic regime. f) A schematic illustration of the experimental setup.

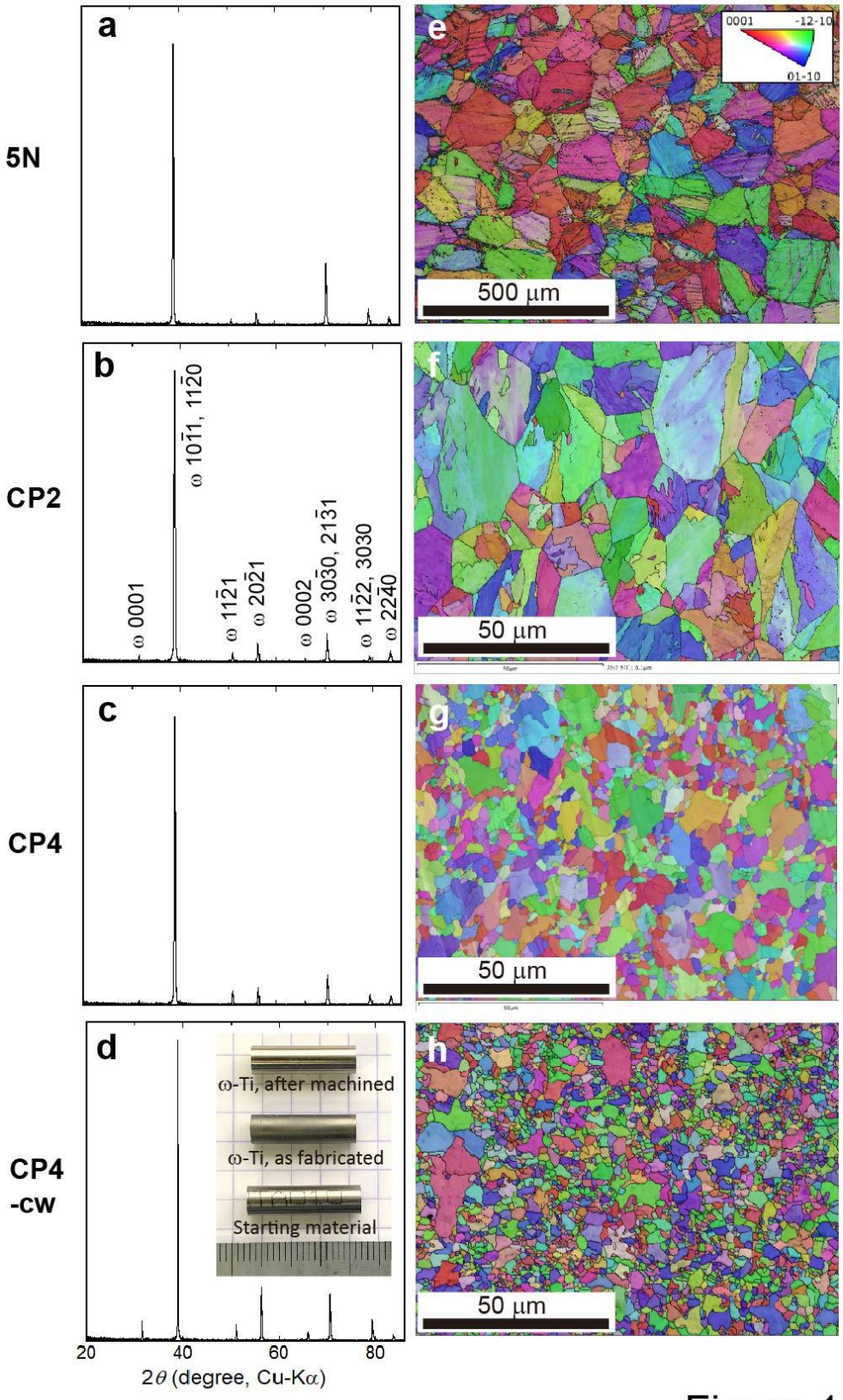
5N
CP2
CP4
CP4
-CW
a
b
c
d
e
f
g
h
ω 0001
ω 10$\bar{1}$1, 11$\bar{2}$0
ω 11$\bar{2}$1
ω 20$\bar{2}$1
ω 0002
ω 30$\bar{3}$0, 21$\bar{3}$1
ω 11$\bar{2}$2, 3030
ω 22$\bar{4}$0
20
40
60
80
2θ (degree, Cu-Kα)
ω-Ti, after machined
ω-Ti, as fabricated
Starting material
0001
-12-10
01-10
500 μm
50 μm
50 μm
50 μm

Figure 1

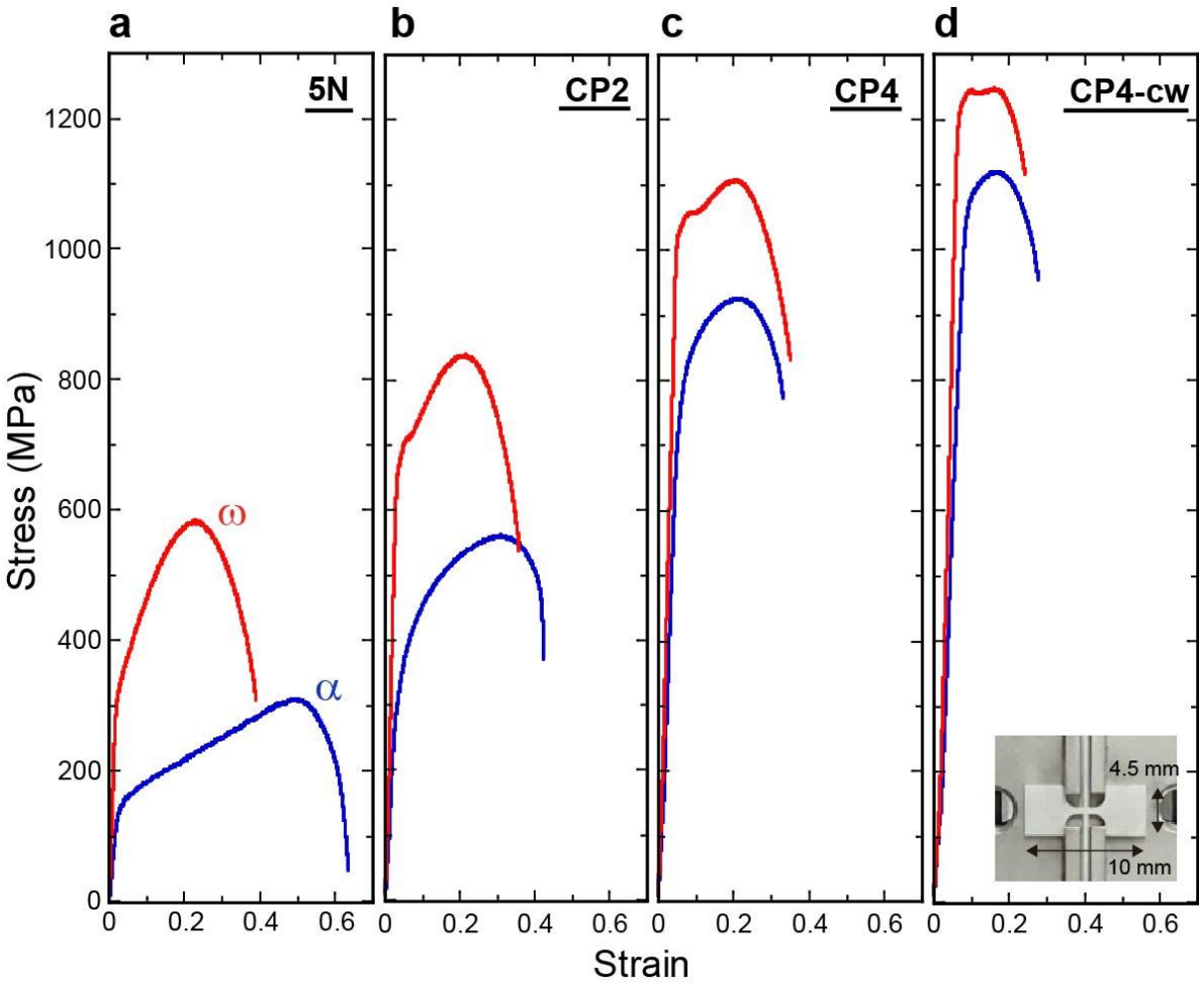

Figure 2

Table 1. Summary of mechanical properties of pure titanium materials determined by miniature tensile tests.

Phase	α				α+β	ω			
Material	5N	CP2	CP4	CP4-cw	Ti64	5N	CP2	CP4	CP4-cw
Grain size (μm)	-	-	-	-	-	65(16)	12(4)	5.2(17)	3.4(11)
$\sigma_{0.2\%}$ (MPa)	118(18)	257(15)	640(50)	973(5)	990(40)	264(9)	634(13)	990(20)	1130(30)
σ_{TS} (MPa)	284(11)	574(14)	930(20)	1121(7)	1190(70)	527(6)	833(11)	1090(30)	1220(30)
ε_f (%)	64(8)	40(2)	28(2)	22(1)	25(3)	38(2)	34(1)	30(2)	16(2)

The averages of the three tensile test runs for each material are shown with one standard deviation in parentheses.
Phase: a phase or phases that are present in the tensile specimens before starting the tensile tests.
5N: 99.999% Ti; CP2: CP-Ti Grade2; CP4: CP-Ti Grade4; CP4-cw; cold-worked CP-Ti Grade4; Ti64: Ti-6Al-4V.
$\sigma_{0.2\%}$: 0.2% offset yield strength; σ_{TS}: tensile strength; ε_f: elongation to failure.

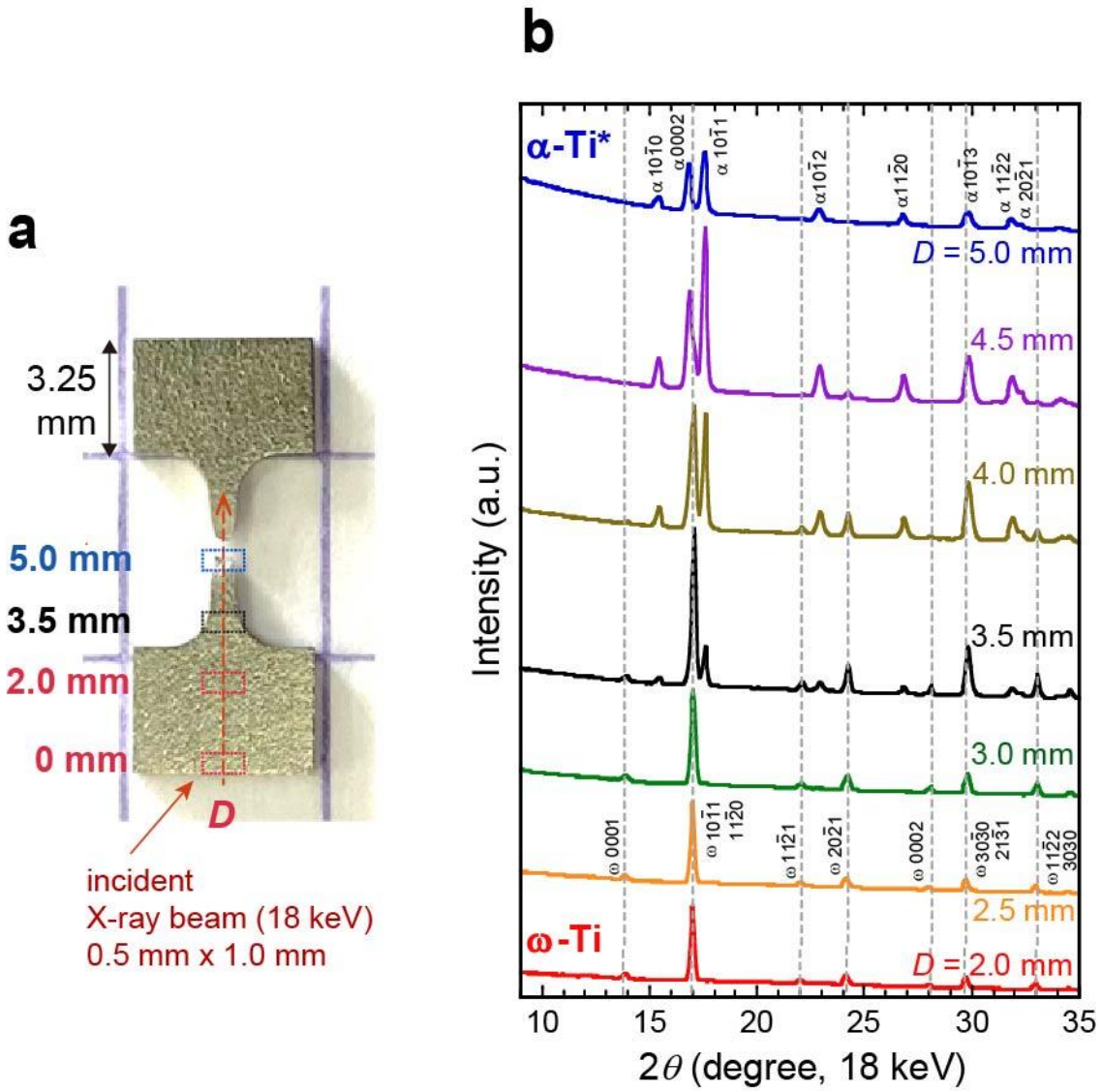
a
3.25 mm
5.0 mm
3.5 mm
2.0 mm
0 mm
D
incident
X-ray beam (18 keV)
0.5 mm x 1.0 mm
b
α-Ti*
α 10$\bar{1}$0
α 0002
α 10$\bar{1}$1
α10$\bar{1}$2
α11$\bar{2}$0
α10$\bar{1}$3
α 11$\bar{2}$2
α 20$\bar{2}$1
D = 5.0 mm
4.5 mm
4.0 mm
3.5 mm
3.0 mm
ω 0001
ω 10$\bar{1}$1
11$\bar{2}$0
ω11$\bar{2}$1
ω 20$\bar{2}$1
ω 0002
ω 30$\bar{3}$0
21$\bar{3}$1
ω11$\bar{2}$2
30$\bar{3}$0
2.5 mm
ω-Ti
D = 2.0 mm
Intensity (a.u.)
10
15
20
25
30
35
2θ (degree, 18 keV)

Figure 3

1
2

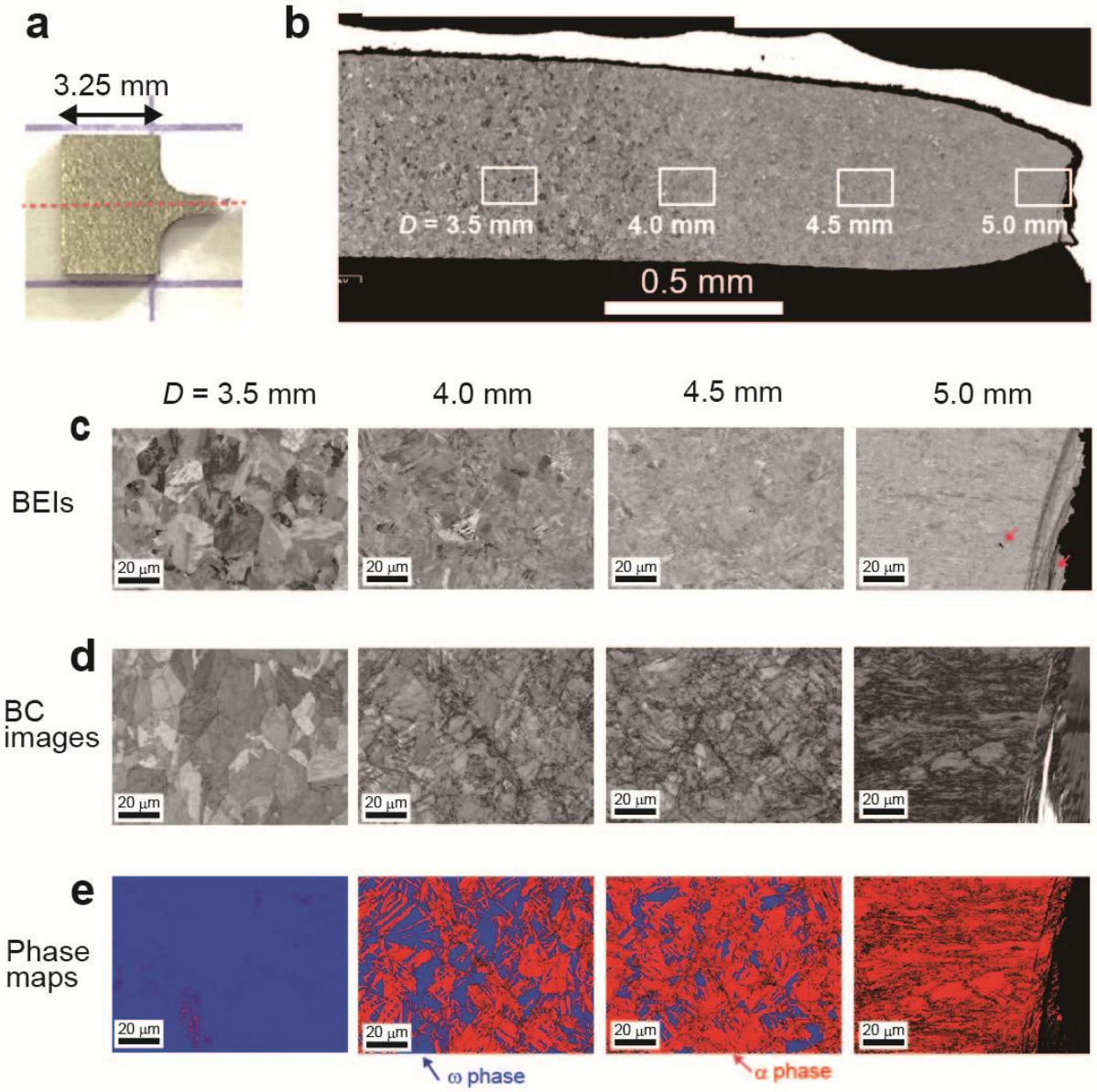
a
3.25 mm
b
D = 3.5 mm
4.0 mm
4.5 mm
5.0 mm
0.5 mm
D = 3.5 mm
4.0 mm
4.5 mm
5.0 mm
c
BEIs
d
BC images
e
Phase maps
20 μm
ω phase
α phase

Figure 4

1

2

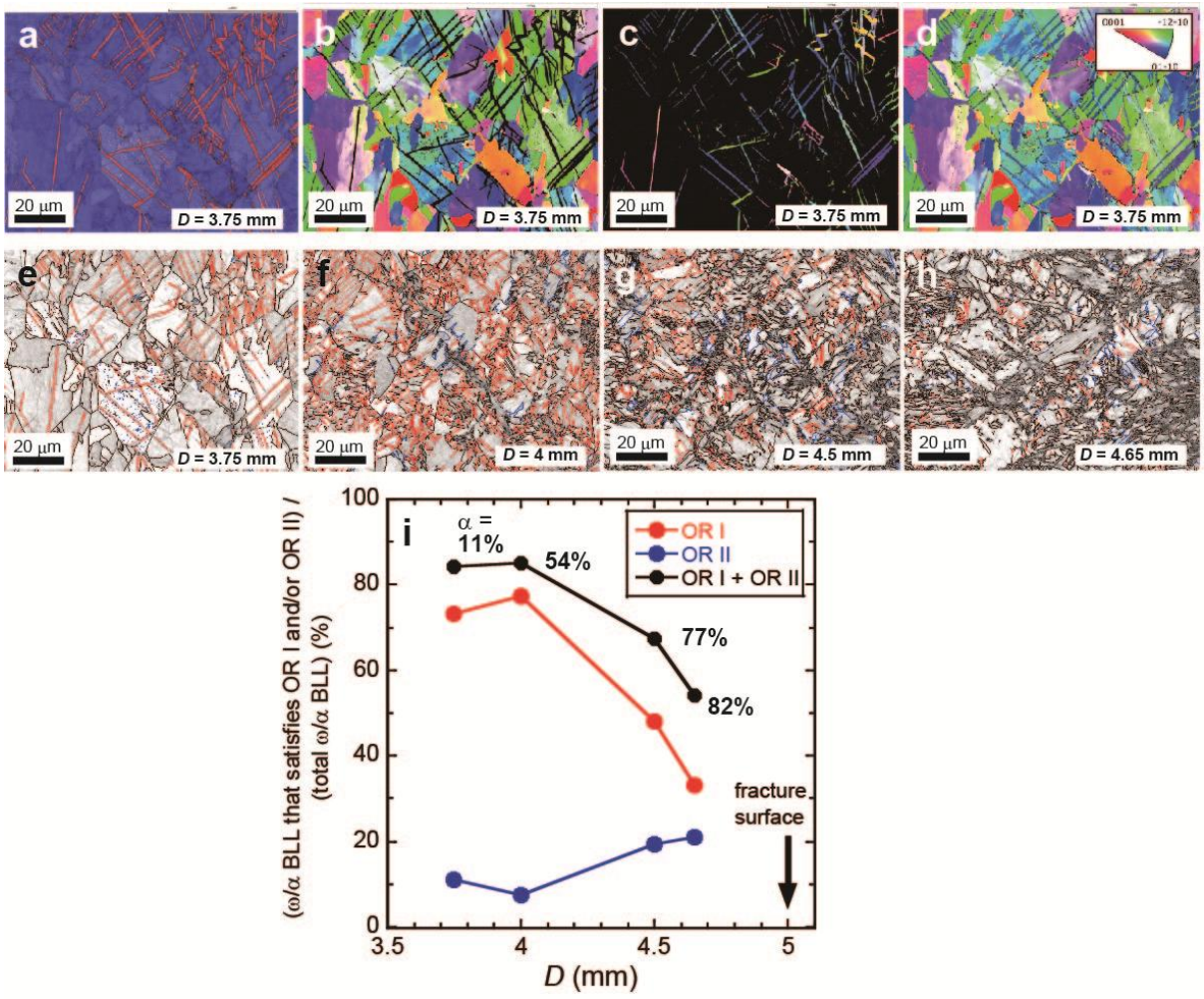
a
b
c
d
e
f
g
h
20 μm
D = 3.75 mm
D = 4 mm
D = 4.5 mm
D = 4.65 mm
i
α = 11%
54%
77%
82%
OR I
OR II
OR I + OR II
fracture surface
(ω/α BLL that satisfies OR I and/or OR II) / (total ω/α BLL) (%)
D (mm)
0
20
40
60
80
100
3.5
4
4.5
5

Figure 5

1

2

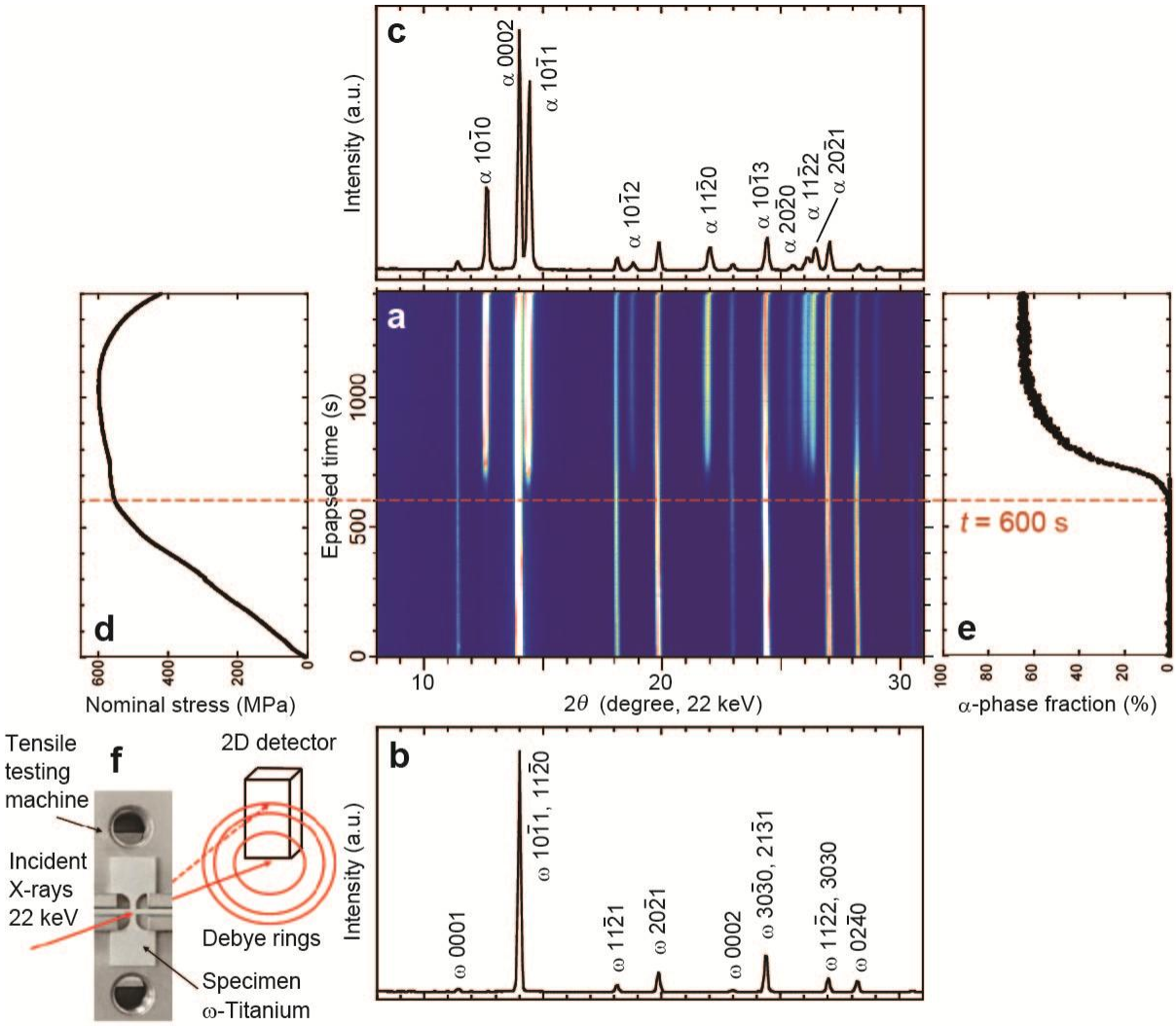
c
Intensity (a.u.)
α 10$\bar{1}$0
α 0002
α 10$\bar{1}$1
α 10$\bar{1}$2
α 11$\bar{2}$0
α 10$\bar{1}$3
α 20$\bar{2}$0
α 11$\bar{2}$2
α 20$\bar{2}$1
a
Epapsed time (s)
0
500
1000
d
Nominal stress (MPa)
600
400
200
0
10
20
30
2θ (degree, 22 keV)
e
t = 600 s
100
80
60
40
20
0
α-phase fraction (%)
Tensile testing machine
f
2D detector
Incident X-rays 22 keV
Debye rings
Specimen ω-Titanium
b
Intensity (a.u.)
ω 0001
ω 10$\bar{1}$1, 11$\bar{2}$0
ω 11$\bar{2}$1
ω 20$\bar{2}$1
ω 0002
ω 30$\bar{3}$0, 21$\bar{3}$1
ω 11$\bar{2}$2, 3030
ω 02$\bar{4}$0

Figure 6